Fractional Envelope Analysis for Rolling Element Bearing Weak Fault Feature Extraction

4 authors:

Jianhong Wang
Nantong University
21 PUBLICATIONS   **133** CITATIONS

SEE PROFILE

Qiao Li-yan
Harbin Institute of Technology
75 PUBLICATIONS   **149** CITATIONS

SEE PROFILE

Yongqiang Ye
Nanjing University of Aeronautics & Astronautics
88 PUBLICATIONS   **996** CITATIONS

SEE PROFILE

YangQuan Chen
University of California, Merced
908 PUBLICATIONS   **23,795** CITATIONS

SEE PROFILE

Some of the authors of this publication are also working on these related projects:

Smart Cave Drone Project View project

Drones View project

Fractional Envelope Analysis for Rolling Element Bearing Weak Fault Feature Extraction

Jianhong Wang, Liyan Qiao, Yongqiang Ye, *Senior Member, IEEE*, and YangQuan Chen, *Senior Member, IEEE*

Abstract—The bearing weak fault feature extraction is crucial to mechanical fault diagnosis and machine condition monitoring. Envelope analysis based on Hilbert transform has been widely used in bearing fault feature extraction. A generalization of the Hilbert transform, the fractional Hilbert transform is defined in the frequency domain, it is based upon the modification of spatial filter with a fractional parameter, and it can be used to construct a new kind of fractional analytic signal. By performing spectrum analysis on the fractional envelope signal, the fractional envelope spectrum can be obtained. When weak faults occur in a bearing, some of the characteristic frequencies will clearly appear in the fractional envelope spectrum. These characteristic frequencies can be used for bearing weak fault feature extraction. The effectiveness of the proposed method is verified through simulation signal and experiment data.

Index Terms—Fractional analytic signal, fractional envelope analysis, fractional Hilbert transform, rolling element bearing, weak fault feature extraction.

I. INTRODUCTION

ROLLING element bearings are at the heart of almost every rotating machine. Therefore, they have received a lot of attention in the field of vibration analysis as they represent a common source of faults, which can be detected at an early stage [1]. Recently, to ensure the reliability and safety of modern large-scale industrial processes, data-driven methods have been receiving considerably increasing attention, particularly for the purpose of process monitoring [2], [3]. The collected vibration data from defective rolling element bearings are generally non-stationary. If processed properly by a fault feature extraction technique, this data can indicate the existence and location of certain faults. However, the vibration signal is still an indirect source of information, as it is often severely corrupted by various noise effects. As a result, the

weak signature is even more difficult to be detected at the early stage of defect development. Its effectiveness in fault feature extraction largely relies on the availability of proper signal processing techniques [4]. A signal feature enhancing method is required to provide more evident information for incipient defect detection of rolling element bearings.

While operating a roller bearing with local faults impulse is created, the high-frequency shock vibration is then generated and the amplitude of vibration is modulated by the pulse force. Therefore resonance demodulation technique provides an important and effective approach to analyze the fault signals of high-frequency impact vibration. Envelope analysis, sometimes known as the high frequency resonance demodulation technique is by far the most successful method for rolling element bearings diagnostics [5]−[9]. At present, the Hilbert transform based envelope analysis has been widely used in rolling element bearings fault diagnosis as one of the most common envelope analysis methods because the characteristic information can be obtained by Hilbert transform, which has quick algorithm and could extract envelope of the rolling element bearings fault vibration signal effectively [10], [11].

However, in the traditional Hilbert transform based envelope analysis method, the fault is identified through the peak value of envelope spectrum. Thus, this traditional method has inherent disadvantages. Fast Fourier transform method is widely used in the spectrum analysis of envelope signals; however, it could only give the global energy-frequency distributions and fail to reflect the details of a signal. So it is hard to analyze a signal effectively when the fault signal is weaker than the interfering signal. At the same time, it is easy to diffuse and truncate the signal's energy as fast Fourier transform regards harmonic signals as basic components, which will lead to energy leakage and cause lower accuracy.

One of the early works in connection with fractional is that of Lohmann *et al.* [12], who proposed two fractional generalizations of the classical Hilbert transform. One definition is a modification of the spatial filter with a fractional parameter, and the other is based on the fractional Fourier transform. In [13], Pei and Yeh developed the discrete version of the fractional Hilbert transform and applied it to the edge detection of images. Tseng and Pei [14] considered optimized design strategies for finite impulse response designs and infinite impulse response models of the discrete-time fractional Hilbert transform, and proposed a novel secure SSB communication application. So far, the research application of fractional Hilbert transform is very young and needs to be explored.

A generalization of Hilbert transform based envelope anal-

ysis, called fractional envelope analysis, is introduced here, which provides a tool to process signal in the fractional Fourier plane instead of a conventional Fourier plane. This method hugs the signal optimally, and could reduce the interference of noise to some extent. Thus, this relatively new signal processing technique has the capability of providing more diagnostic information than conventional Hilbert transform based envelope analysis. Reference [5] describes that the Kurtosis value is very sensitive to bearing fault signal. Therefore, the Kurtosis is feasible to be the index for selecting the optimal fractional order envelope analysis.

The remainder of the paper is organized as follows: Section II presents necessary theoretical background of Hilbert transform. The fractional envelope analysis based upon the modification of spatial filter with a fractional parameter is introduced in Section III. Simulations and experimental validations are performed consequently in Sections IV and V. Conclusions are drawn in Section VI.

II. HILBERT TRANSFORM

The Hilbert transform of the function $x(t)$ is defined by an integral transform [11], [15]:

$$H[x(t)] = \hat{x}(t) = \frac{1}{\pi} \int_{-\infty}^{\infty} \frac{x(\tau)}{t - \tau} d\tau. \tag{1}$$

Because of a possible singularity at $t = \tau$, the integral has to be considered as a Cauchy principal value. Mathematically, the Hilbert transform $\hat{x}(t)$ of the original function represents a convolution of $x(t)$ and $1/(\pi t)$, which can be written as:

$$\hat{x}(t) = x(t) * \left(\frac{1}{\pi t} \right). \tag{2}$$

Note that the Hilbert transform of a time-domain signal $x(t)$ is another time-domain signal $\hat{x}(t)$. If $x(t)$ is real-valued, then so is $\hat{x}(t)$. The transfer function of Hilbert transform becomes

$$H_1(\omega) = -j\mathrm{sgn}(\omega) = \begin{cases} -j, & \omega > 0 \\ 0, & \omega = 0 \\ j, & \omega < 0. \end{cases} \tag{3}$$

Physically, the Hilbert transform can be viewed as a filter of unity amplitude and phase $\pm 90°$ depending on the sign of the frequency of the input signal spectrum. The Hilbert filter takes an input signal and returns the Hilbert transform of the signal as an output signal. This is also referred to as a Hilbert transformer, a quadrature filter, or a $90°$ phase shifter.

III. FRACTIONAL ENVELOPE ANALYSIS

Note that the Heaviside step function, or unit step function, is defined by [12], [15]:

$$H(\omega) = \frac{1}{2}(1 + \mathrm{sgn}(\omega)) = \begin{cases} 1, & \omega > 0 \\ \frac{1}{2}, & \omega = 0 \\ 0, & \omega < 0. \end{cases} \tag{4}$$

Equation (3) can be rewritten in terms of the Heaviside step function as follows:

$$H_1(\omega) = -jH(\omega) + jH(-\omega). \tag{5}$$

Equation (5) can be put in the following form:

$$H_1(\omega) = \exp\left(-j\frac{\pi}{2}\right) H(\omega) + \exp\left(j\frac{\pi}{2}\right) H(-\omega). \tag{6}$$

A fractional generalization of this result can be written as follows:

$$H_p(\omega) = \exp\left(-jp\frac{\pi}{2}\right) H(\omega) + \exp\left(jp\frac{\pi}{2}\right) H(-\omega). \tag{7}$$

This can be conveniently rewritten as

$$H_p(\omega) = \cos\left(p\frac{\pi}{2}\right) - j\mathrm{sgn}(\omega)\sin\left(p\frac{\pi}{2}\right) \tag{8}$$

or

$$H_p(\omega) = \cos\left(p\frac{\pi}{2}\right) H_0(\omega) + \sin\left(p\frac{\pi}{2}\right) H_1(\omega). \tag{9}$$

In fact, the transfer function of Hilbert transform (3) can be written as

$$H_1(\omega) = -j\mathrm{sgn}(\omega)$$

$$= \begin{cases} \exp\left(-j\frac{\pi}{2}\right), & \omega > 0 \\ \dfrac{\exp\left(-j\frac{\pi}{2}\right) + \exp\left(j\frac{\pi}{2}\right)}{2}, & \omega = 0 \\ \exp\left(j\frac{\pi}{2}\right), & \omega < 0. \end{cases} \tag{10}$$

We introduce the kth-order Hilbert operator $H_k = H^k$ to represent the kth-repetition of the Hilbert transform. Thus, the Fourier transform of the kth-order Hilbert transform can be expressed as

$$F[H_k x(t)] = F(\omega) \cdot [-j\mathrm{sgn}(\omega)]^k. \tag{11}$$

The formula (11) can be generalized to a non-integer p and the transfer function of the pth-order Hilbert operator H_p is

$$H_p(\omega) = [-j\mathrm{sgn}(\omega)]^p$$

$$= \begin{cases} \exp\left(-jp\frac{\pi}{2}\right), & \omega > 0 \\ \dfrac{\exp\left(-jp\frac{\pi}{2}\right) + \exp\left(jp\frac{\pi}{2}\right)}{2}, & \omega = 0 \\ \exp\left(jp\frac{\pi}{2}\right), & \omega < 0. \end{cases} \tag{12}$$

This can be conveniently rewritten as (8). Thus, the pth-order Hilbert operator H_p can be expressed as

$$H_p = \cos\left(p\frac{\pi}{2}\right) \cdot I + \sin\left(p\frac{\pi}{2}\right) \cdot H_1 \tag{13}$$

where $H_0 = I$ is the identity operator. The pth-order Hilbert transform is

$$\hat{x}(t) = H_p[x(t)] = \cos\left(p\frac{\pi}{2}\right) \cdot x(t) + \sin\left(p\frac{\pi}{2}\right) \cdot H_1(t). \tag{14}$$

The parameter p is called the order. The above definition of fractional Hilbert transform is a weighted sum of the original signal and its conventional Hilbert transform, and it is based upon modifying the spatial filter with fractional parameter. The magnitude response and the phase response are

$$|H_p(\omega)| = 1 \tag{15}$$

and

$$\varphi(\omega) = \begin{cases} -p\frac{\pi}{2}, & \omega > 0 \\ p\frac{\pi}{2}, & \omega < 0 \end{cases} \tag{16}$$

respectively.

Fig. 1 shows the block diagram for implementing the generalized fractional Hilbert transform.
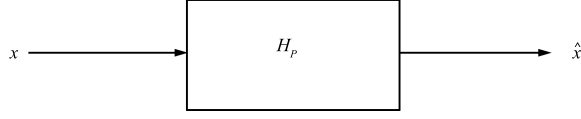

Fig. 1. Block diagram for implementation of the generalized fractional Hilbert transform.

As we know, Fourier transform is fundamental tool in fractional-order systems and controls [16]. In fact, among Hilbert, fractional Hilbert, and fractional calculus there are the following transfer function, magnitude response, and phase response relations (Table I).

TABLE I
COMPARISON OF HILBERT, FRACTIONAL HILBERT, AND FRACTIONAL CALCULUS

	Hilbert	Fractional Hilbert	Fractional calculus
Transfer	$-i\text{sgn}(\omega)$	$[-i\text{sgn}(\omega)]^p$	$(i\omega)^{\nu}$
Magnitude	1	1	$|\omega|^{\nu}$
Phase	$-\frac{\pi}{2}\text{sgn}(\omega)$	$-\frac{p\pi}{2}\text{sgn}(\omega)$	$\frac{\nu\pi}{2}\text{sgn}(\omega)$

From Table I, the phase characteristic of the fractional calculus operator ($\nu = -p$) is the same as the phase characteristic of the fractional Hilbert. However, the fractional calculus operator is actually a singular low-pass ($\nu < 0$) filter, or a singular high-pass ($\nu > 0$) filter (Fig. 2), although the fractional Hilbert is an all-pass filter.
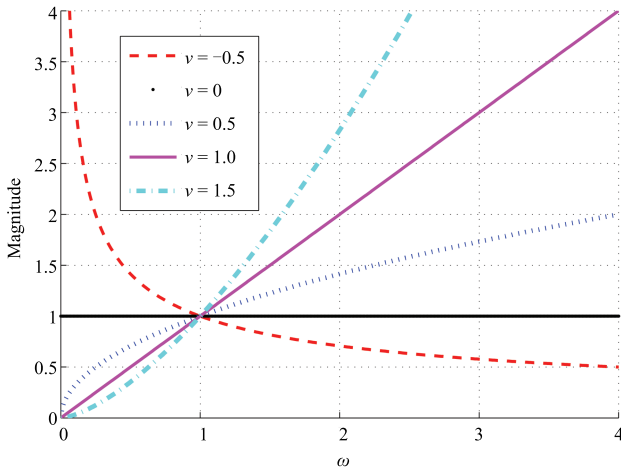

Fig. 2. Magnitude response of the fractional calculus operator.

The real signal $x(t)$ and its fractional Hilbert transform $\hat{x}(t)$ can form a new complex signal, which is called the fractional analytical signal, such that

$$y(t) = x(t) + j\hat{x}(t). \qquad (17)$$

The envelope $A(t)$ of the complex signal $y(t)$ is defined as

$$A(t) = |x(t) + j\hat{x}(t)| = \sqrt{x^2(t) + \hat{x}^2(t)}. \qquad (18)$$

The application to fractional envelope analysis is shown in Fig. 3 [5]. Fig. 3 depicts the envelope as the modulus of the analytic signal obtained by inverse transformation of the selected one-sided frequency band.
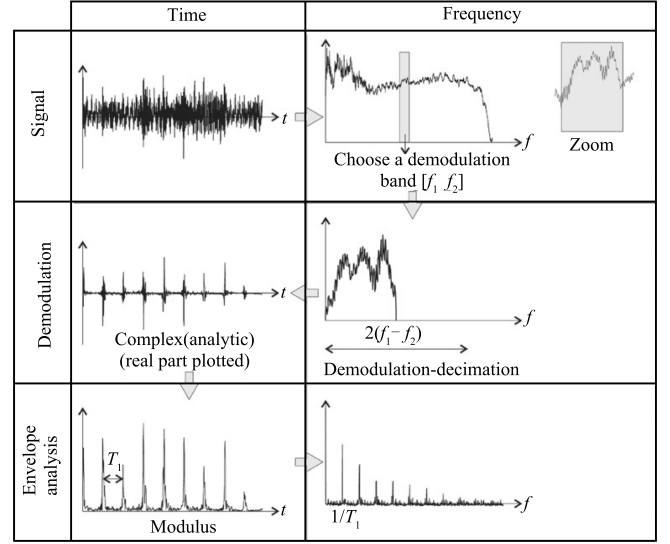

Fig. 3. Procedure for envelope analysis using the fractional Hilbert transform method.

By performing spectrum analysis on the envelope signal $A(t)$, the fractional envelope spectrum can be obtained. When faults occur on a bearing, some of the characteristic frequencies will clearly appear in the fractional envelope spectrum. These characteristic frequencies can be used for bearing weak fault feature extraction.

The algorithm for rolling element bearing fractional envelope analysis consists of the following steps:

Step 1: Rolling element bearing vibration signal acquisition.

Step 2: Taking fractional Hilbert transform of vibration signal.

Step 3: Taking magnitude of fractional analytical signal to obtain fractional envelope signal.

Step 4: Taking fast Fourier transform (FFT) of fractional envelope signal.

Step 5: Analyzing envelope spectrum at bearing fault frequencies.

IV. SIMULATION ANALYSIS

In this section, a simple simulation is used to illustrate the fractional envelope characteristic of the bearing fault signal with strong background noise. The bearing system including the transducer is simplified as a single degree of freedom (SDOF) system and the vibration induced by a single defect in the rolling element bearing can be given by [8]

$$x(t) = \sum_{k=0}^{+\infty} A_k e^{-\xi\omega_n(t-T_k)} \times \sin(\omega_n(t-T_k)) \qquad (19)$$

where ω_n denotes the resonance angular frequency of the system and $\omega_n = 2\pi f_n$, where f_n denotes the resonance frequency. The amplitude of the kth transient response A_k

is set to be 5, the sampling frequency f_s is 20 kHz, the resonance frequency f_n of system is 3 kHz, the maximal slip ratio of its period T is 0.01 s, the relative damping ratio ξ is 0.1. The profile of a typical signal, contaminated with -2 dB additive Gaussian noise, (i.e., SNR $= -2$), is shown in Fig. 4. Figs. 4 (a) and 4 (b) display the time waveform of the original signal and noisy signal. The frequency spectrum of the noisy signal is shown in Fig. 4 (c). It is hard to reveal some useful information from Fig. 4 (c). Therefore, the proposed method is used to achieve the enhancement of fault detection.
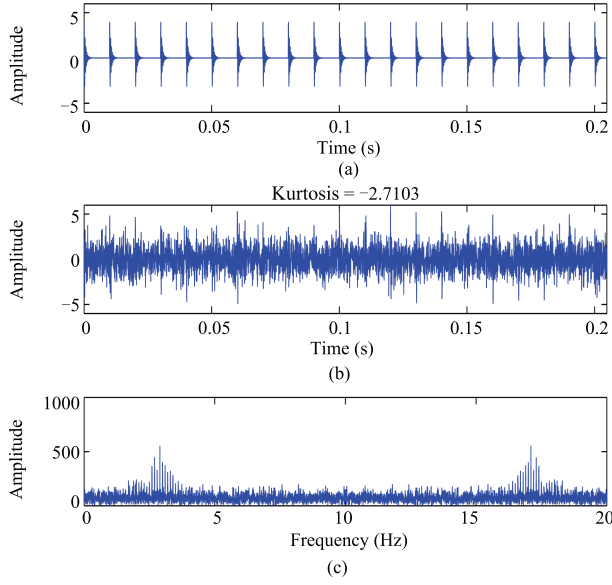

Fig. 4. Simulated signal: (a) time waveform of original signal, (b) time waveform of signal contaminated with -2 dB additive Gaussian noise and (c) frequency spectrum waveform.

As a matter of fact, the Kurtosis has often been employed in the signal processing community to solve "blind" problems: blind identification and equalisation of systems by output Kurtosis maximisation, blind separation of mixed signals by individual maximisation of the source Kurtosis, etc [17]. Here, the sample version of the Kurtosis (20) is used to blindly identify the optimal order of fractional Hilbert transformer. This Kurtosis is taken as the normalised fourth order moment given by [5]

$$K = \frac{m_4}{m_2^2} = \frac{\frac{1}{N}\sum_{i=1}^{N}(x_i - \bar{x})^4}{\left(\frac{1}{N}\sum_{i=1}^{N}(x_i - \bar{x})^2\right)^2} \tag{20}$$

where m_4 is the fourth sample moment about the mean, m_2 is the second sample moment about the mean (sample variance), N is the number of samples, x_i is the ith sample and $\bar{x}$ is the sample mean. For symmetric unimodal distributions, positive Kurtosis indicates heavy tails and peakedness relative to the normal distribution, whereas negative Kurtosis indicates light tails and flatness [18].

Table II presents the comparison of Kurtosis using different order Hilbert transformer filtering simulation signal (19) contaminated with -2 dB additive white Gaussian noise. Note

that, 0.2-order is suitable for this envelope spectrum analysis. For this reason, our method has larger design flexibility than the integer (1-order) Hilbert transform-based method. The 0.2-order envelope signal and 0.2-order envelope spectrum of the 0.2-order Hilbert transformer filtered signal are shown in Fig. 5. It can be seen that in Fig. 5 (b) the characteristic frequencies clearly appear in the 0.2-order envelope spectrum. These characteristic frequencies can be used for bearing fault diagnosis.

TABLE II
COMPARISON OF KURTOSIS BETWEEN DIFFERENT ORDER
HILBERT TRANSFORM

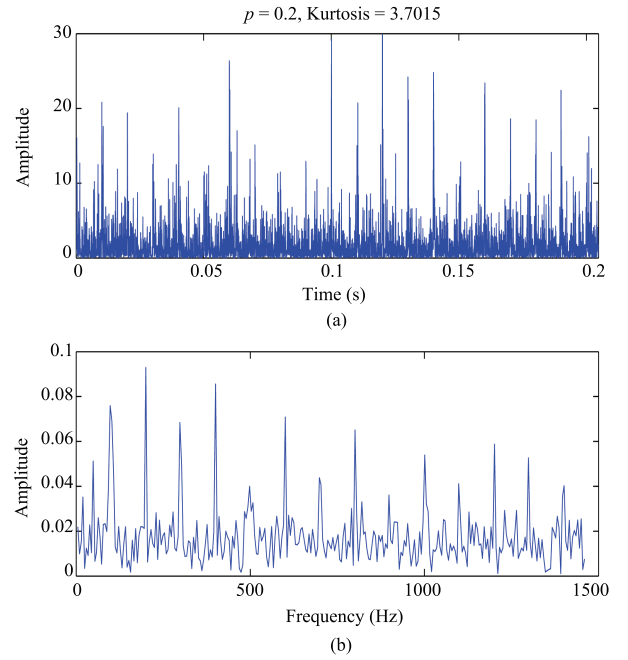| Order	0	0.1	0.2	0.3	0.4
Kurtosis	3.0461	3.3907	3.7015	3.5582	2.9891
0.5	0.6	0.7	0.8	0.9	1.0
2.5702	2.7531	3.1859	3.3133	3.0536	2.7558

Fig. 5. Envelope spectrum obtained by the 0.2-order Hilbert transform.

V. EXPERIMENTAL VALIDATION

The success of the proposed method in detecting early defect under strong additive stationary noise is clearly demonstrated in the above simulation. In this section, the application to actual vibration signals collected in a rolling element bearing accelerated life test is presented.

Generally, the vibration spectrum of a healthy bearing contains only the information related to the shaft rotation speed and its harmonics, which is shown as Zone I in Fig. 6. Any other frequencies might indicate noise, or frequencies related to other rotating parts operating at the same time with the bearing under test [19]. A rolling element bearing fault could appear at the outer, the inner race and (or) on the rolling elements. During its early stages, the damage on the surface is mostly only localized. The vibration signal in this case

includes repetitive impacts of the moving components on the defect. These impacts might create repetition frequencies that depend on whether the defect is on the outer or the inner race, or on the rolling element (Fig. 7).
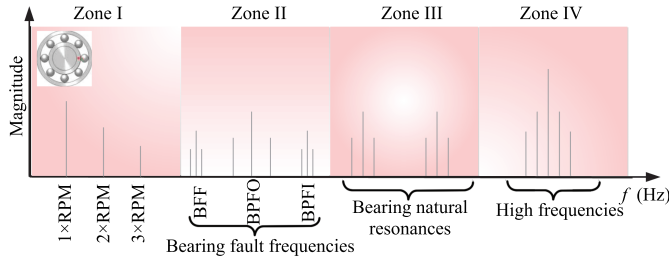

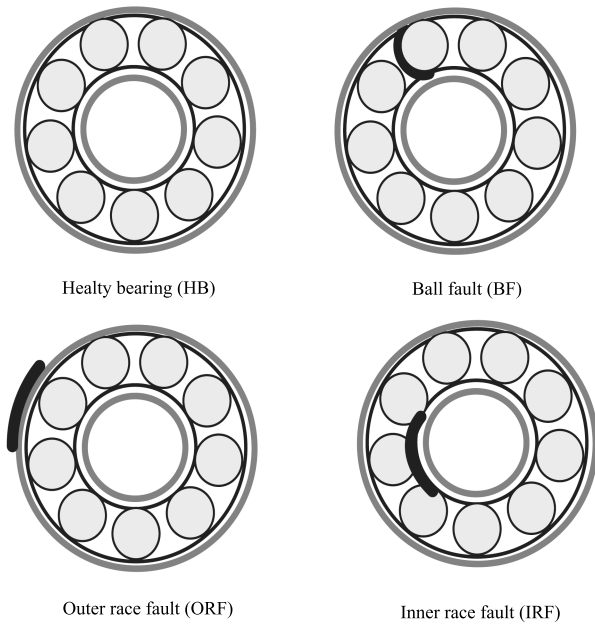Fig. 6. Frequency content of a vibration signal of a damaged rolling element bearing.

Fig. 7. A series of bearing components with faults induced in them indicated in bold line [20].

The repetition rates are denoted bearing frequencies. The formulae for the ball passing frequency outer (BPFO) race, ball passing frequency inner (BPFI) race, and ball fault frequency (BFF) are as follows [5]:

$$f_{\text{BPFO}} = \frac{n}{2} f_r \left(1 - \frac{d}{D} \cos \theta \right)$$

$$f_{\text{BPFI}} = \frac{n}{2} f_r \left(1 + \frac{d}{D} \cos \theta \right)$$

$$f_{\text{BFF}} = \frac{D}{2d} f_r \left[1 - \left(\frac{d}{D} \cos \theta \right)^2 \right] \qquad (21)$$

where n is the number of rolling elements, f_r is the shaft rotational frequency (RPM), d is the diameter of rolling element, (i.e., ball) diameter, D is the pitch diameter, and θ is the angle of the load from the radial plane.

For early faults, the repetition impulses could create initially an increase of frequencies in the high frequency range (Zone IV), and may excite the resonant frequencies of the bearing parts later in Zone III, as well as the repetition frequencies of Zone II (BPFO, BPFI, BFF).

The vibration signals collected in the bearing center of case western reserve university (CWRU) [21] are used to illustrate the fractional envelope analysis. The test stand consists of a 2 hp drive induction motor, a torque transducer/encoder, a dynamometer, and control electronics (Figs. 8 and 9). The test bearings which support the motor shaft have single point faults with the diameters of 0.007 inch, 0.014 inch, 0.021 inch, and 0.028 inch on the outer race, inner race, and ball of the drive end bearings produced by an electro-discharge machine. Faulted bearings were reinstalled into the test motor and vibration data was recorded for motor loads of 0 to 3 horsepower (motor speeds of 1797 to 1720 rpm). The number n of rolling elements is 9 and the angle θ of the load from the radial plane is $0°$. Vibration data was collected using a 16 channel DAT recorder at 12 000 samples per second. The bearing is a deep groove ball bearing and the model is 6205-2RS JEM SKF. The diameter and depth of the pit are 0.18 mm and 0.28 mm respectively. The geometry (outside diameter, inside diameter, thickness, ball diameter, and pitch diameter) and defect frequencies of the bearing are listed in Tables III and IV.
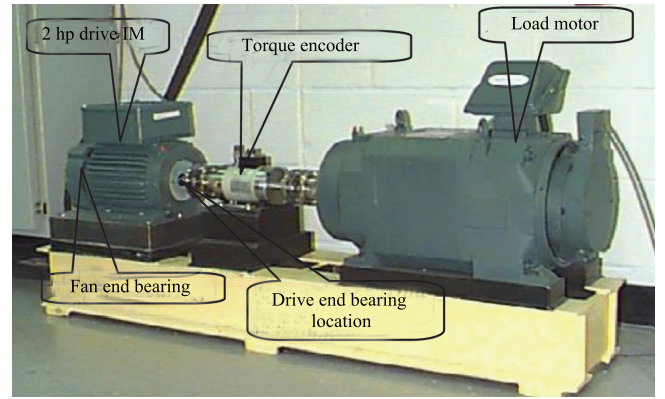

Fig. 8. Experimental test rig, composed of a 2 hp drive induction motor, a torque transducer/encoder, load [21].
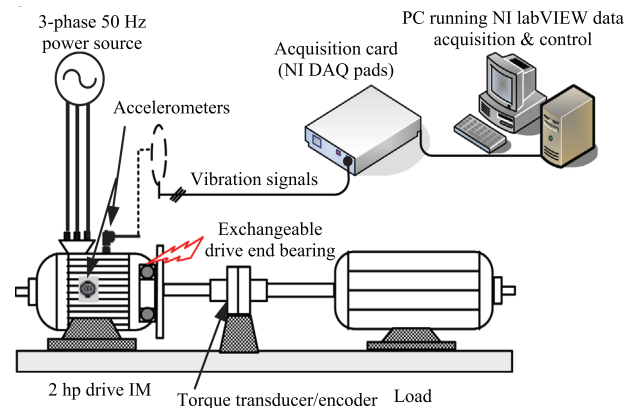

Fig. 9. Schematic of the experimental test rig [22].

TABLE III
SIZE OF ROLLING ELEMENT BEARING (MM)

Type	Outside	Inside	Thickness	Ball	Pitch
SKF6025	51.9989	25.0012	15.0012	7.9400	39.0398

TABLE IV
DEFECT FREQUENCIES OF ROLLING ELEMENT BEARING,
(MULTIPLE OF RUNNING SPEED)

Type	Outer ring	Inner ring	Rolling element
SKF6025	3.5848	5.4152	4.7135

A. Case 1: Outer Race Fault

The outer race fault is located at the 6 o'clock position and the accelerometer is attached to the housing with a magnetic base. In this case, the shaft frequency f_r is 29.17 Hz (1750/60, shaft rotates at the speed of 1750 rpm). The characteristic bearing defect frequency f_{BPFO} is equal to 3.5848 times the shaft rotation speed based on (21). Thus, the fault characteristic frequency f_{BPFO} is 104.56 Hz.

Fig. 10 (a) gives the temporal waveform of outer race fault diameter of 0.007 inch. Fig. 10 (b) shows the corresponding optimal fractional (0.1-order, Table V) envelope spectrum. The fault characteristic frequency f_{BPFO} is located at 105 Hz, and its associated harmonics, at 209.8 Hz, 314.8 Hz, 419.7 Hz, and so on, can be easily detected.
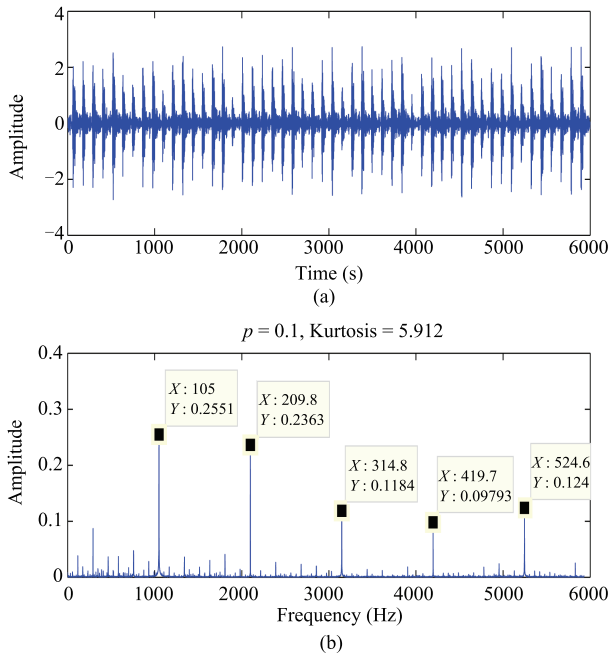

Fig. 10. The temporal waveform of the signal of OR007@6-2 and the corresponding envelope spectrum obtained by the 0.1-order Hilbert transform.

B. Case 2: Inner Race Fault

In this case, the shaft frequency f_r is 29.13 Hz (shaft rotates at the speed of 1748 rpm). The characteristic bearing defect frequency f_{BPFI} is equal to 5.4152 times the shaft rotation speed based on (22). Thus, the fault characteristic frequency f_{BPFI} is 157.76 Hz.

TABLE V
COMPARISON OF KURTOSIS BETWEEN DIFFERENT ORDER
HILBERT TRANSFORM

Order	0	0.1	0.2	0.3	0.4
Kurtosis	5.8875	5.9120	5.8019	5.3508	4.2234
	0.5	0.6	0.7	0.8	0.9	1.0
	3.0349	1.3953	0.4235	0.3769	0.9572	1.8214

Fig. 11 (a) gives the temporal waveform of inner race fault diameter of 0.007 inch and the corresponding optimal fractional (0.5-order, Table VI) envelope spectrum is shown in Fig. 11 (b). It can be seen that the $1\times$, $2\times$, $3\times$ BPFI are very clear in Fig. 11 (b).
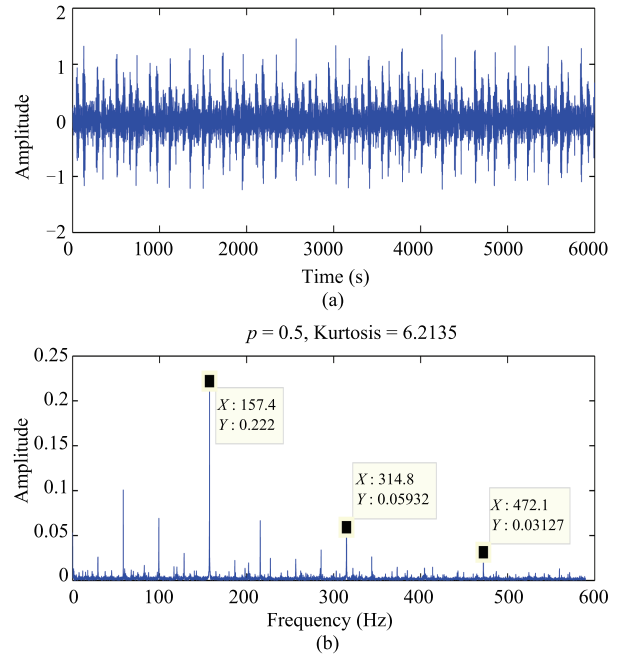

Fig. 11. The temporal waveform of the signal of IR007-2 and the corresponding envelope spectrum obtained by the 0.5-order Hilbert transform.

TABLE VI
COMPARISON OF KURTOSIS BETWEEN DIFFERENT ORDER
HILBERT TRANSFORM

Order	0	0.1	0.2	0.3	0.4
Kurtosis	4.7495	4.7805	4.7163	4.2787	3.1397
	0.5	0.6	0.7	0.8	0.9	1.0
	6.2135	0.4184	0.4780	1.1967	1.6665	1.6513

C. Case 3: Ball Fault

In this case, the shaft frequency f_r is 29.13 Hz (shaft rotates at the speed of 1748 rpm). The characteristic bearing defect frequency f_{BFF} is equal to 4.7135 times the shaft rotation speed based on (23). Thus, the fault characteristic frequency f_{BFF} is 137.30 Hz.

Fig. 12 (a) gives the temporal waveform of ball fault diameter of 0.028 inch. It can be seen that there are many obvious periodic impulses in Fig. 12 (a), which may be caused by the interaction between the faulty parts and connected rolling

element surfaces. In order to obtain clear fault information, the corresponding optimal fractional (0.9-order, Table VII) envelope spectrum is shown in Fig. 12 (b). It can be seen that the characteristic frequencies are $1\times$, $2\times$, $3\times$ BFF and its harmonics modulated by f_r (Fig. 6), which implies the occurrence of ball fault. Moreover, there are some frequency components in Fig. 12 (b). The fault information can hardly be obtained from single fractional envelope analysis without prior filtration. The possible reason for other frequency components may be that the signals collected are usually disturbed by the nearby bearings or other background noise [19].
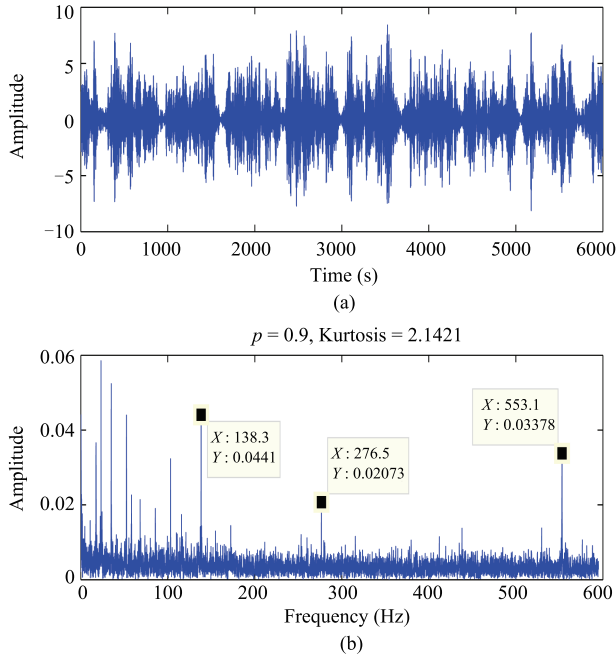

Fig. 12.   The temporal waveform of the signal of B028-2 and the corresponding envelope spectrum obtained by the 0.9-order Hilbert transform.

TABLE VII
COMPARISON OF KURTOSIS BETWEEN DIFFERENT ORDER
HILBERT TRANSFORM

Order	0	0.1	0.2	0.3	0.4
Kurtosis	1.9349	1.9552	1.9037	1.5660	0.6402
0.5	0.6	0.7	0.8	0.9	1.0
0.9391	1.0778	1.4084	1.7998	2.1421	1.0845

Figs. $10-12$ altogether show that the proposed fractional Hilbert transform based envelop analysis provides better envelop detection results and achieves better Kurtosis performance than the envelop analysis based on traditional Hilbert transform on the studied bearing fault signals. These results demonstrate the excellent compromise capability of the fractional Hilbert transformer in detect accuracy and filtering noisy bearing fault signal. This method may therefore serve as an effective framework for the model-based detection of noisy rolling element bearings.

VI. CONCLUSION

The fractional Hilbert transform signal detect model based upon the modification of spatial filter with a fractional pa-

rameter technique is constructed in this work, which breaks the thought that the traditional fault detect model can only be based on integer-order Hilbert transform. By setting a flexible fractional order, our model can better enhance the compromise capability in detect accuracy and filtering noisy bearing fault signal. The effectiveness of the method is demonstrated on both simulated signal and actual data are collected in rolling bearing accelerated life test. The proposed technique exhibits excellent performances on visual sense and quantitative comparison. While the cyclic frequency error has some influence on the performance of the proposed method, how to reduce the cyclic frequency error and extract the coupled faults are worthy of further study.

REFERENCES

[1] N. Sawalhi, R. B. Randall, and H. Endo, "The enhancement of fault detection and diagnosis in rolling element bearings using minimum entropy deconvolution combined with spectral kurtosis," *Mech. Syst. Signal Process.*, vol. 21, no. 6, pp. 2616−2633, Aug. 2007.

[2] S. Yin, S. X. Ding, X. C. Xie, and H. Luo, "A review on basic data-driven approaches for industrial process monitoring," *IEEE Trans. Ind. Electron.*, vol. 61, no. 11, pp. 6418−6428, Nov. 2014.

[3] B. P. Cai, Y. H. Liu, Q. Fan, Y. W. Zhang, Z. K. Liu, S. L. Yu, and R. J. Ji, "Multi-source information fusion based fault diagnosis of ground-source heat pump using Bayesian network," *Appl. Energy*, vol. 114, pp. 1−9, Feb. 2014.

[4] W. Sun, G. A. Yang, Q. Chen, A. Palazoglu, and K. Feng, "Fault diagnosis of rolling bearing based on wavelet transform and envelope spectrum correlation," *J. Vib. Control*, vol. 19, no. 6, pp. 924−941, Apr. 2013.

[5] R. B. Randall and J. Antoni, "Rolling element bearing diagnostics-a tutorial," *Mech. Syst. Signal Process.*, vol. 25, no. 2, pp. 485−520, Feb. 2011.

[6] Y. Ming, J. Chen, and G. M. Dong, "Weak fault feature extraction of rolling bearing based on cyclic Wiener filter and envelope spectrum," *Mech. Syst. Signal Process.*, vol. 25, no. 5, pp. 1773−1785, Jul. 2011.

[7] P. Borghesani, P. Pennacchi, and S. Chatterton, "The relationship between kurtosis- and envelope-based indexes for the diagnostic of rolling element bearings," *Mech. Syst. Signal Process.*, vol. 43, no. 1−2, pp. 25−43, Feb. 2014.

[8] A. B. Ming, W. Zhang, Z. Y. Qin, and F. L. Chu, "Envelope calculation of the multi-component signal and its application to the deterministic component cancellation in bearing fault diagnosis," *Mech. Syst. Signal Process.*, vol. 50−51, pp. 70−100, Jan. 2015.

[9] R. H. Jiang, S. L. Liu, Y. F. Tang, and Y. H. Liu, "A novel method of fault diagnosis for rolling element bearings based on the accumulated envelope spectrum of the wavelet packet," *J. Vib. Control*, vol. 21, no. 8, pp. 1580−1593, Jun. 2015.

[10] M. Feldman, "Hilbert transform in vibration analysis," *Mech. Syst. Signal Process.*, vol. 25, no. 3, pp. 735−802, Apr. 2011.

[11] M. Feldman, *Hilbert Transform Applications in Mechanical Vibration*. Chichester, UK: John Wiley and Sons, 2011.

[12] A. W. Lohmann, D. Mendlovic, and Z. Zalevsky, "Fractional Hilbert transform," *Opt. Lett.*, vol. 21, no. 4, pp. 281−283, Feb. 1996.

[13] S. C. Pei and M. H. Yeh, "Discrete fractional Hilbert transform," *IEEE Trans. Circ. Syst. II: Analog Digit. Signal Process.*, vol. 47, no. 11, pp. 1307−1311, Nov. 2000.

[14] C. C. Tseng and S. C. Pei, "Design and application of discrete-time fractional Hilbert transformer," *IEEE Trans. Circ. Syst. II: Analog Digit. Signal Process.*, vol. 47, no. 12, pp. 1529−1533, Dec. 2000.

[15] F. W. King, *Hilbert Transforms*. Cambridge, UK: Cambridge University Press, 2009.

[16] C. A. Monje, Y. Q. Chen, B. M. Vinagre, D. Y. Xue, and V. Feliu, *Fractional-order Systems and Controls: Fundamentals and Applications*. London, UK: Springer, 2010.

[17] J. Antoni and R. B. Randall, "The spectral Kurtosis: Application to the vibratory surveillance and diagnostics of rotating machines," *Mech. Syst. Signal Process.*, vol. 20, no. 2, pp. 308−331, Feb. 2006.

[18] L. T. DeCarlo, "On the meaning and use of kurtosis," *Psychol. Methods*, vol. 2, no. 3, pp. 292−307, Sep. 1997.

[19] L. Saidi, J. B. Ali, and F. Fnaiech, "The use of spectral kurtosis as a trend parameter for bearing faults diagnosis," in *Proc. 15th Int. Conf. Sciences and Techniques of Automatic Control and Computer Engineering*, Hammamet, Tunisia, 2014, pp. 394−399.

[20] L. Saidi, J. B. Ali, and F. Fnaiech, "Bi-spectrum based-EMD applied to the non-stationary vibration signals for bearing faults diagnosis," *ISA Trans.*, vol. 53, no. 5, pp. 1650−1660, Sep. 2014.

[21] K. A. Loparo, Bearings vibration data set. Case Western Reserve University. [Online]. Available: http://csegroups.case.edu/bearingdatacenter/pages/12k-drive-end-bearing-fault-data.

[22] L. Saidi, J. B. Ali, and F. Fnaiech, "Application of higher order spectral features and support vector machines for bearing faults classification," *ISA Trans.*, vol. 54, pp. 193−206, Jan. 2015.

Liyan Qiao received the B. S. degree in radio engineering from Harbin Institute of Technology, China, in 1992, the M. S. degree in communication and electronics system from Harbin Institute of Technology, China, in 1996, and the Ph. D. degree in instrumentation science and technology from Harbin Institute of Technology, China, in 2005. He is at the Automatic Test and Control Faculty of School of Electrical Engineering and Automation, Harbin Institute of Technology, Harbin, China. His research interests include automatic test system, data acquiring technic through internet, flash storage system, and signal analysis.

Yongqiang Ye received the B. S. and M. S. degrees from Zhejiang University, China, in 1994 and 1997, respectively, and the Ph. D. degree from Nanyang Technological University, Singapore, in 2004, all in electrical engineering. He had been a faculty member with the School of Information, Zhejiang University of Finance and Economics, China, for more than four years. He had also been a postdoctoral fellow with the Department of Electrical Engineering at Lakehead University, the Department of Systems and Computer Engineering at Carleton University, and the Department of Mechanical Engineering, Dalhousie University, Canada, respectively. He joined the Department of Automation Engineering at Nanjing University of Aeronautics and Astronautics in 2009 as a professor. He is a Senior Member of IEEE. His research interests include computer vision, pattern recognition, learning and repetitive control, and power electronics control.

Jianhong Wang received the B. S. degree in mathematics and applied mathematics from Jiangsu Normal University, China, in 2000, the M. S. degree in operations research and control theory from Shanghai Jiao Tong University, China, in 2007, and the Ph. D. degree in control theory and control engineering from Nanjing University of Aeronautics and Astronautics, China, in 2016. He was a visiting scholar with the School of Engineering at the University of California, Merced, USA, in 2015. He is currently an associate professor at the School of Science, Nantong University, China. His current research interests include applied fractional calculus in intelligent control, signal processing, image processing, and big data processing. Corresponding author of this paper.

YangQuan Chen received his Ph. D. degree in advanced control and instrumentation from Nanyang Technological University, Singapore, in 1998. Dr. Chen was on the Faculty of Electrical and Computer Engineering at Utah State University before he joined the School of Engineering, University of California, Merced in 2012 where he teaches "Mechatronics" for juniors and "Fractional Order Mechanics" for graduates. His current research interests include mechatronics for sustainability, cognitive process control and hybrid lighting control, multi-UAV based cooperative multi-spectral "personal remote sensing" and applications, applied fractional calculus in controls, signal processing and energy informatics; distributed measurement and distributed control of distributed parameter systems using mobile actuator and sensor networks.